An Active Inductor-Based VCO With Wide Tuning Range and High DC-to-RF Power Efficiency

Jiangtao Xu, *Student Member, IEEE*, Carlos E. Saavedra, *Senior Member, IEEE*, and Guican Chen

***Abstract*—An active inductor-based voltage-controlled oscillator (VCO) with a wide frequency tuning range was designed and fabricated using a standard 0.13-μm CMOS process. The oscillator has an LC-tank topology with cross-coupled transistors, and the active inductor was realized using a pair of fully differential very high-speed operational transconductance amplifiers. Due to the differential nature of the inductor, the even harmonics of the output signal were much reduced. Measured results show that the VCO is tunable from 833 MHz to 3.72 GHz, representing a tuning range of 127%. The VCO can produce -0.9 dBm of radio-frequency power. The core circuit, excluding output buffers, consumes 13 mW from a 1.2-V supply.**

***Index Terms*—Active inductor, feedback resistance, high-linearity high-speed operational transconductance amplifier (OTA), high output power, voltage-controlled oscillator (VCO), wide tuning range.**

I. Introduction

THE RECOGNITION that active inductor-based voltage-controlled oscillators (VCOs) can have exceptionally wide frequency tuning ranges, exceeding 100%, and that they can be optimized to consume small amounts of power has sparked a good amount of interest in these circuits over the last several years [1]–[4]. Another incentive to explore the use of active inductors in VCOs are the savings in chip space relative to using physical inductors, particularly when a large inductance is required at relatively low frequencies.

In this brief, we present a VCO circuit that uses a differential active inductor. The active inductor is based on a gyrator-C topology with very high-speed operational transconductance amplifiers (OTAs) as the constituent building blocks. By using a differential active inductor, the VCO can handle large signals and produce -0.9 dBm of output power, which is quite high for a CMOS oscillator. According to the definition of the phase noise, high output carrier power means low phase noise at the same phase noise power level. The chip core consumes maximum power of 13 mW, resulting in a direct-current (dc)-to-radio-frequency (RF) power efficiency value of 6.3%, which to our knowledge is the highest reported to date for an active inductor-based VCO and is comparable with the power efficiency of a VCO using a physical LC tank.

Manuscript received November 15, 2010; revised January 25, 2011, March 8, 2011 and April 8, 2011; accepted May 2, 2011. Date of publication July 5, 2011; date of current version August 17, 2011. This paper was recommended by Associate Editor H. Barthelemy.

J. Xu is with the School of Electronics and Information, Xi'an Jiaotong University, Xi'an 710049, China, and also with Queen's University, Kingston, ON K7L 3N6, Canada (e-mail: rfic.xu@gmail.com).

C. E. Saavedra is with the Department of Electrical and Computer Engineering, Queen's University, Kingston, ON K7L 3N6, Canada.

G. Chen is with the School of Electronics and Information, Xi'an Jiaotong University, Xi'an 710049, China.

Color versions of one or more of the figures in this paper are available online at http://ieeexplore.ieee.org.

Digital Object Identifier 10.1109/TCSII.2011.2158713

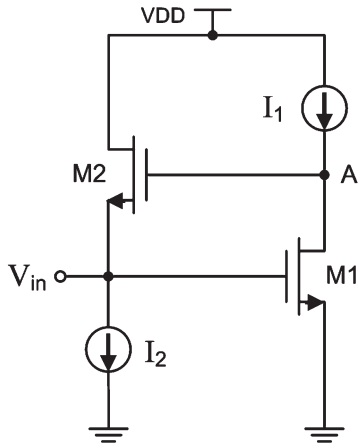

Fig. 1. Simple single-ended gyrator-C active inductor.

II. Active Inductor Design

A. Basic Concepts

A commonly used active inductor topology is depicted in Fig. 1, which consists of two transistors that are arranged to function as an impedance-inverting network. The gyrator inverts the total capacitance at node A to the inductive impedance at input terminal $V_{\rm in}$. If $V_{\rm ov}$ is the overdrive voltage, and $V_{\rm sat}$ is the voltage required by the current source I_1 in Fig. 1, then the voltage swing at the input node will be limited between voltages $V_T + V_{\rm ov}$ and $VDD - V_T - V_{\rm sat} - V_{\rm ov}$, where V_T is the threshold voltage of the transistors. Using this active inductor in an LC-tank oscillator has the potential advantage of low dc power consumption but, on the other hand, since the voltage swing of the circuit at the inductor node is confined to a small range of values, the RF output power of the oscillator would be correspondingly limited. Furthermore, when cascode and regulated cascode topologies are employed to reduce the equivalent series resistance and enhance the Q-factor as usual, the voltage swing will be further degraded.

A differential active inductor has the following three key advantages over a single-ended one: 1) the voltage swing of differential active inductors can be twice as large than that of a comparable single-ended active inductor; 2) as with any differential configuration, the circuit will reject the common-mode disturbances of the system and suppress the even-order harmonics; and 3) the need for a 50% duty cycle in most oscillators calls for differential topologies.

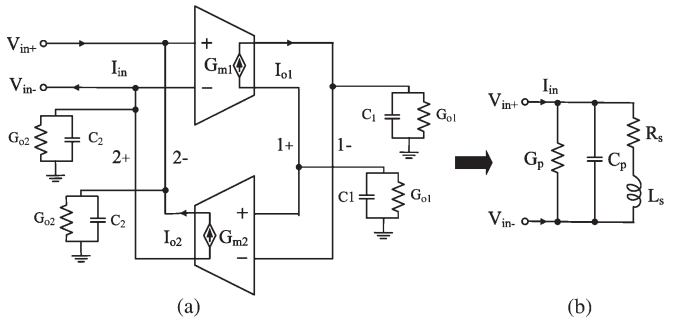

Fig. 2. Schematic of (a) a differential active inductor and its (b) equivalent circuit.

By replacing the two transistors in Fig. 1 with a pair of differential-input/differential-output OTAs [5], it is possible to make a differential active inductor. The resulting gyrator circuit is shown in Fig. 2(a), and it includes the input and output conductance and capacitance values of the OTAs. An equivalent circuit of the differential active inductor is shown in Fig. 2(b), and the component values are given by

$$G_p = \frac{G_{o2}}{2} \tag{1}$$

$$C_p = \frac{C_2}{2} \tag{2}$$

$$R_s = \frac{G_{o1}}{2G_{m1}G_{m2}} \tag{3}$$

$$L_s = \frac{C_1}{2G_{m1}G_{m2}} \tag{4}$$

where G_{o1} is the total shunt conductance, and C_1 is the total shunt capacitance at the differential node 1. Similarly, G_{o2} and C_2 are the total shunt conductance and capacitance, respectively, at differential node 2. The expressions for the conductance and capacitance values are $G_{o1} = g_{o1} + g_{i2}$, $G_{o2} = g_{o2} + g_{i1}$, $C_1 = C_{o1} + C_{i2}$, and $C_2 = C_{o2} + C_{i1}$, where $g_{i,n}$ and $g_{o,n}$ are the input and output conductance values of OTA$_n$, respectively, and capacitors $C_{i,n}$ and $C_{o,n}$ denote the input and output capacitance values of OTA$_n$, respectively. Neglecting R_s in Fig. 2(b), the self-resonant frequency can be easily shown to be

$$\omega_o = \frac{1}{\sqrt{L_s C_p}} = 2\sqrt{\frac{G_{m1}}{C_1}\frac{G_{m2}}{C_2}} = 2\sqrt{\omega_{t1}\omega_{t2}} \tag{5}$$

where $\omega_{t1} = G_{m1}/C_1$ and $\omega_{t2} = G_{m2}/C_2$ are the cutoff frequencies of OTA$_1$ and OTA$_2$, respectively. This self-resonant frequency is typically the maximum frequency at which the active inductor operates.

B. Active Inductor With Resistive Feedback

To reduce the series resistance R_s in Fig. 2(b), a feedback resistor, i.e., R_f, can be inserted into the gyrator, as shown in Fig. 3 [6], [7]. We can use the same equivalent circuit as before, and while the expressions for parallel conductance G_p and capacitance C_p remain unchanged, the equations for R_s and L_s are now

$$G_p = \frac{G_{o2}}{2} \tag{6}$$

$$C_p = \frac{C_2}{2} \tag{7}$$

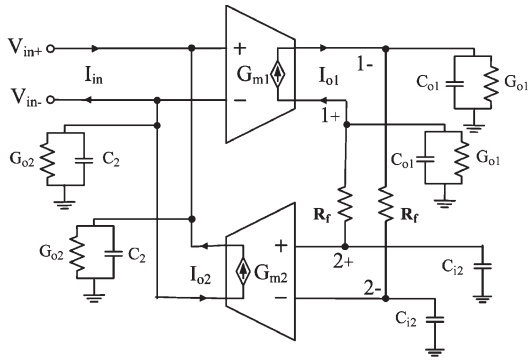

Fig. 3. Floating active inductor with resistive feedback.

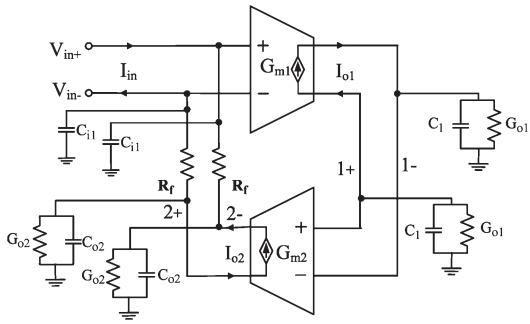

Fig. 4. Proposed differential active inductor with resistive feedback at the input.

$$R_s = \frac{G_{o1} - \omega^2 C_{o1} C_{i2} R_f}{2G_{m1}G_{m2}} \tag{8}$$

$$L_s = \frac{C_{o1} + C_{i2}(1 + G_{o1}R_f)}{2G_{m1}G_{m2}}. \tag{9}$$

Next, by changing the location of R_f to the input side of the gyrator, as shown in Fig. 4, the performance of the active inductor can be significantly improved, as will be explained shortly. In this last configuration, the component values of the equivalent circuit are

$$G_p = \frac{G_{o2}}{2}\frac{1}{1 + R_f G_{o1}} \tag{10}$$

$$C_p = \frac{C_{i1}}{2} \tag{11}$$

$$R_s = \frac{G_{o1} + G_{o1}G_{o2}R_f - \omega^2 C_1 C_{o2} R_f}{2G_{m1}G_{m2}} \tag{12}$$

$$L_s = \frac{C_1(1 + G_{o2}R_f) + C_{o2}G_{o1}R_f}{2G_{m1}G_{m2}}. \tag{13}$$

Comparing (6)–(9) with (10)–(13), we reach the following conclusions about the performance of the two circuits.

1) Equivalent parallel conductance G_p is reduced by a factor of $1/(1 + R_f G_{o1})$.
2) Equivalent parallel capacitance C_p is reduced by $C_{o2}/2$.
3) The inductance of L_s is increased by the factor

$$1 + \frac{2C_{o1}G_{o1}R_f}{C_{o1} + C_{i2}(1 + G_{o1}R_f)}. \tag{14}$$

The circuits in Figs. 3 and 4 were simulated using identical OTAs in order to compare their equivalent inductances, and the results are shown in Figs. 5 and 6. The imaginary part X of

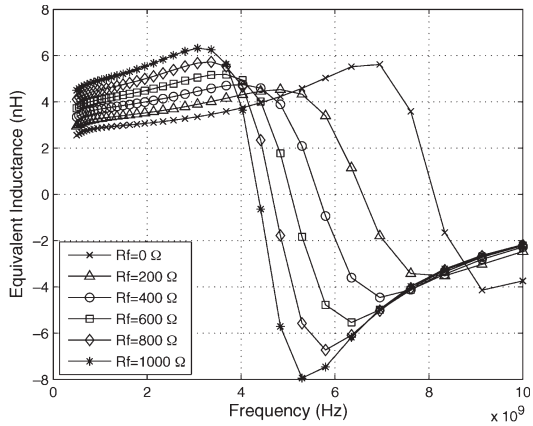

Fig. 5. Simulated equivalent inductance of the circuit in Fig. 3.

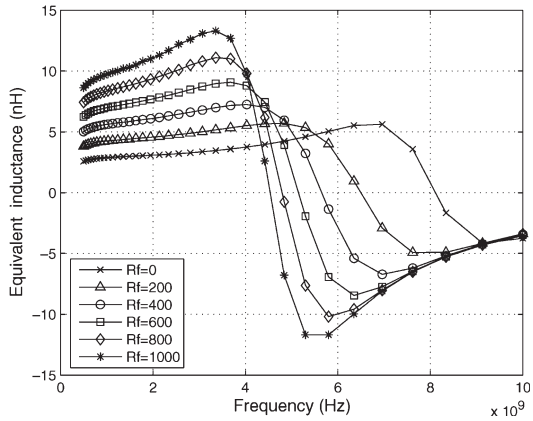

Fig. 6. Simulated inductance of the proposed gyrator in Fig. 4.

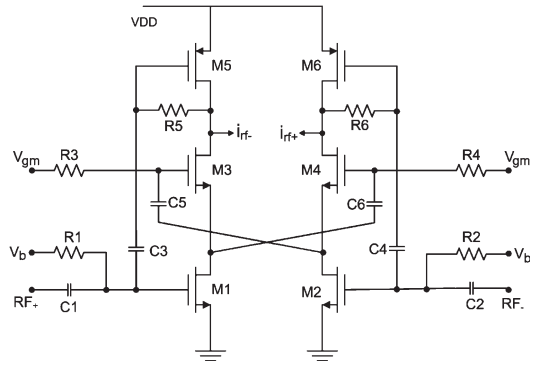

Fig. 7. High-linearity high-speed OTA.

input impedance $(R + jX)$ is used here to derive the equivalent inductance (X/ω) of the active inductors. Due to the effect of C_p in Fig. 2(b), at certain frequencies, X transits from positive into negative. As predicted in (14), we observe that at 2 GHz, the active inductor in Fig. 5 exhibits an inductance range from 3 to 5.5 nH, whereas the proposed circuit in Fig. 6 has an inductance in the enlarged range of 3–11 nH.

C. OTA

The schematic of the OTA used in this design is shown in Fig. 7. The OTA is a low-power very wideband circuit that uses an active inductor load. The nMOS-only feedforward-regulated cascode topology makes it more appropriate for the low supply voltage while retaining high-linearity and high-speed performance [8]–[10]. $V_{\rm gm}$ is the control voltage to tune the transconductance of the OTA. We analyze the linearity of the OTA by observing the G_m variation versus the magnitude of differential input voltage signal $V_{\rm in}$. G_m compresses as $V_{\rm in}$ increases. Fig. 8 shows the normalized transconductance of the OTA versus the magnitude of the RF input signal at $V_{\rm gm} = 0.7$ V. Normalization is relative to $G_{\rm m.max}$, which is the transconductance obtained under small input signal conditions at the lowest measurement frequency of 500 MHz. From 500 MHz to 4 GHz, G_m decreases by 0.12 dB, which represents a 1.4% reduction. The input 1-dB compression point for G_m is 0.56 V at 4 GHz and 0.62 V at 500 MHz, which means that the OTA can handle a larger signal at its input port than the simple one shown in Fig. 1.

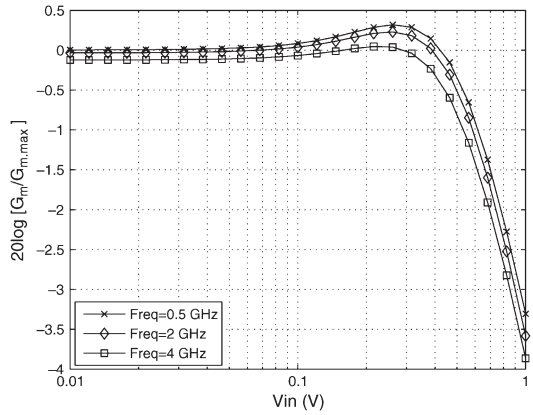

Fig. 8. Linearity of the high-speed OTA.

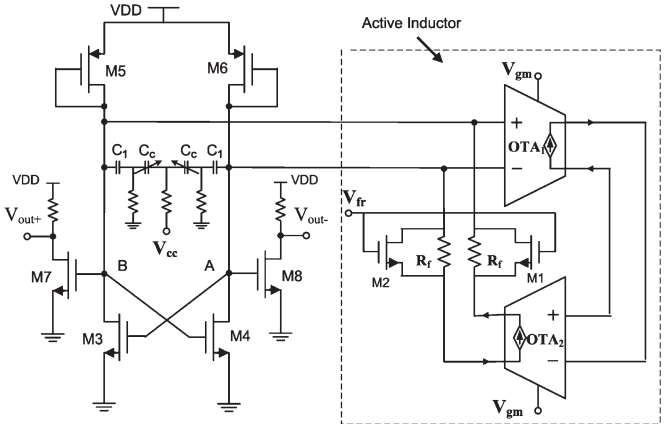

Fig. 9. Full schematic of the active inductor-based VCO.

III. Design of Active Inductor-Based Oscillator

The complete schematic of the proposed active inductor-based VCO is shown in Fig. 9. The LC-tank consists of the tunable active inductor and the varactor for coarse and fine frequency tunings, respectively. The transconductance of the OTA is controlled by $V_{\rm gm}$, and the capacitance of the varactor is controlled by $V_{\rm cc}$. Transistor M1 in parallel with constant resistor R_f is used as a variable feedback resistance controlled by $V_{\rm fr}$. As $V_{\rm fr}$ increases, the feedback resistance decreases, and the oscillation frequency increases. The cross-coupled nMOS transistor pair M3/M4 provides negative conductance that is in parallel with the LC tank. To ensure that oscillation initiates, the negative conductance should be sufficiently large to

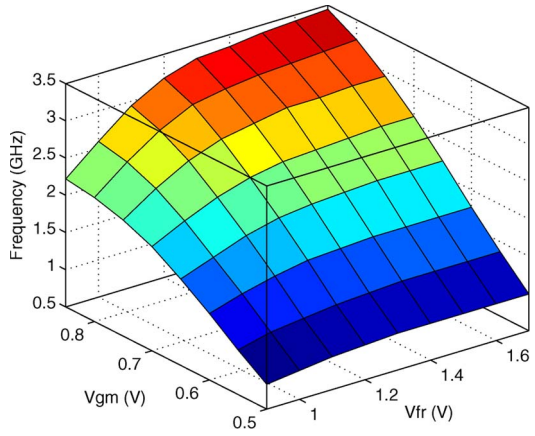

Fig. 10. Measured frequency tuning characteristics versus $V_{\rm gm}$ and $V_{\rm fr}$.

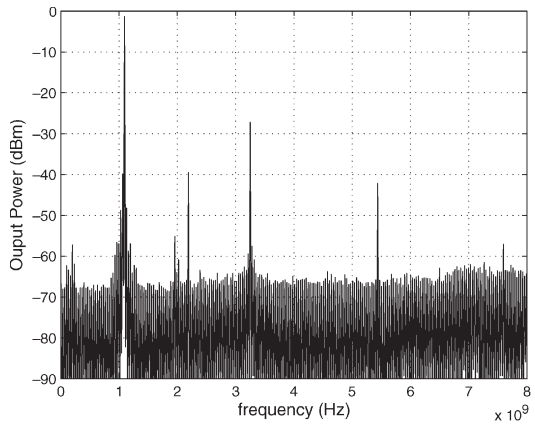

Fig. 11. Measured output harmonic spectra at 1 GHz.

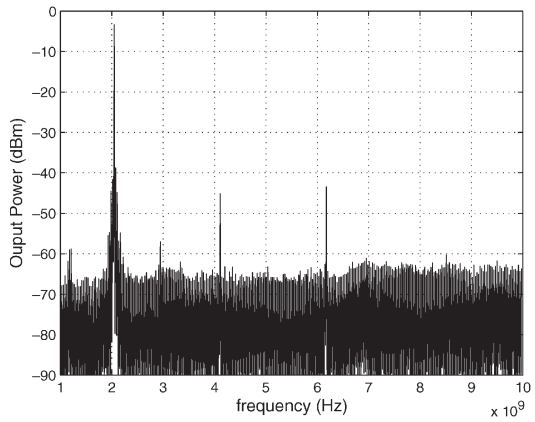

Fig. 12. Measured output harmonic spectra at 2 GHz.

compensate the loss of the active inductor. According to the rule-of-thumb for the VCO design, the negative conductance is chosen three times larger than the largest parallel conductance. An output buffer is employed at the output port for measurement purpose. Its output port is matched to 50 Ω, and its gain is set to 0 dB in simulation to remove its effect on the output power.

Now, we have three dimensions of tuning flexibility, i.e., tuning the transconductance values of the OTAs via $V_{\rm gm}$, tuning the feedback resistance to change the inductance via $V_{\rm fr}$, and tuning the varactor to change the capacitance via $V_{\rm cc}$. From the analysis above, larger transconductance of the OTA results in

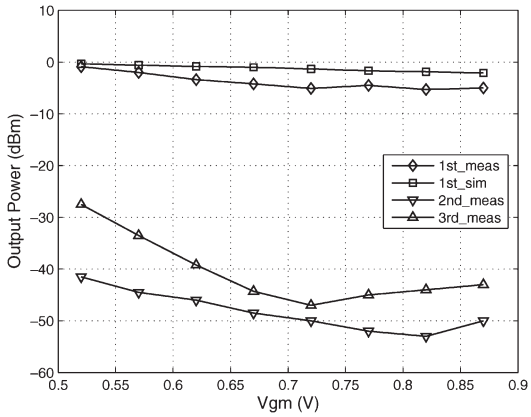

Fig. 13. Harmonic output power values versus $V_{\rm gm}$.

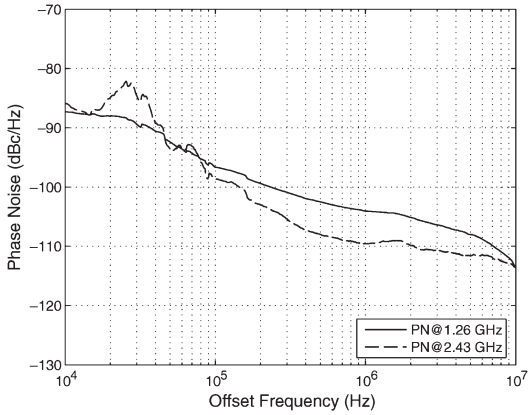

Fig. 14. Measured phase noise at 1.26 and 2.43 GHz.

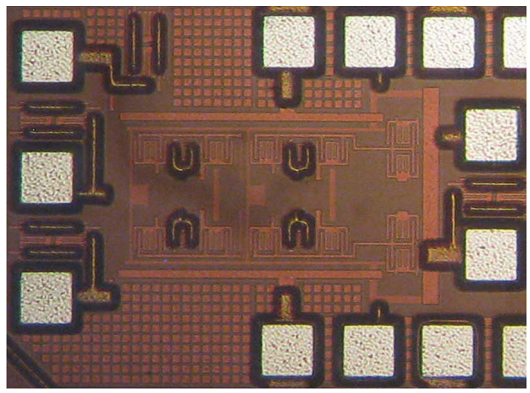

Fig. 15. Microphotograph of the fabricated active inductor-based VCO.

smaller active inductance; larger feedback resistance results in larger active inductance. The bias voltage of the varactor can be tuned from -0.5 to 1 V, which corresponds to a capacitance value of 120–330 fF. Therefore, the proposed oscillator resonates at the highest possible frequency when $V_{\rm gm} = 0.87$ V, $V_{\rm rf} = 1.7$ V, and $V_{\rm cc} = -0.5$ V.

Furthermore, the OTAs are connected via alternating-current coupling and do not share the same dc operating point. Therefore, comparing with the simple active inductor consisting of two back-to-back transistors, the proposed design can handle larger signals without obviously associated nonlinearity. The input dynamic range of the active inductor is in accordance with the input linearity of the OTAs. In addition, this is why high output power can be obtained in this design.

TABLE I
PERFORMANCE SUMMARY AND COMPARISON TABLE

Reference	Technology	Tuning Range	% Tuning	Power Consumption	Output Power	Power Efficiency	Phase Noise
This work	0.13μm Si CMOS	0.83 GHz$\sim$ 3.72 GHz	127%	13 mW (max)	-0.9 dBm to -5 dBm	6.25%	-104 to -109 dBc/Hz @ 1 MHz offset
[2]	0.18μm Si CMOS	0.5 GHz$\sim$ 3.0 GHz	143%	28 mW (max)	-14 dBm to -22 dBm	0.14%	-101 to -118 dBc/Hz @ 1 MHz offset
[1]	0.18μm Si CMOS	1.3 GHz$\sim$ 3.8 GHz	98.04%	5mW	-15 dBm to -10 dBm	2%	-81 to -94 dBc/Hz @ 1 MHz offset
[3]	0.18μm Si CMOS	0.5 GHz$\sim$ 2.0 GHz	120%	13.8mW	-21 dBm to -19 dBm	0.09%	-78 to -90 dBc/Hz @ 1 MHz offset
[3]	0.13μm SiGe BiCMOS	1.6 GHz$\sim$ 5.1 GHz	104 %	2.7 mW	-20 dBm to -18 dBm	0.59%	-85 to -93 dBc/Hz @ 1 MHz offset
[4]	0.35μm Si CMOS	100 MHz$\sim$ 900 MHz	160 %	-	-22 dBm to -11 dBm	-	-86 to -102 dBc/Hz @ 500 kHz offset
[11]	0.13μm Si CMOS	5.5 GHz$\sim$ 9.2 GHz	50.3 %	31 mW (max)	-20 dBm	0.032%	-95 to -114 dBc/Hz @ 1 MHz offset

IV. EXPERIMENTAL RESULTS

The proposed active inductor-based oscillator was fabricated in a standard 0.13-μm CMOS process, and the chip measures $400\ \mu\text{m} \times 270\ \mu\text{m}$ excluding bonding pads. To reduce the noise in the control path, large by-pass capacitors are included on-chip for the dc pads.

As V_{gm} is tuned from 0.5 to 0.87 V and V_{fr} from 0.9 to 1.7 V, the fabricated VCO exhibits a coarse frequency tuning range from 833 MHz to 3.445 GHz, which is slightly narrower than the simulation result of 0.8–3.6 GHz. Fig. 10 shows the detailed frequency tuning characteristics for a constant varactor voltage V_{cc} of 1 V.

Further measurements reveal that as V_{cc} is swept from 1 V to -0.5 V when $V_{\text{gm}} = 0.87$ V and $V_{\text{fr}} = 1.7$ V, the VCO exhibits a fine frequency tuning range from 3.445 to 3.725 GHz. Spectral measurements were taken for fundamental output frequencies of 1 and 2 GHz, and the results are shown in Figs. 11 and 12, respectively. We see in both cases that the even-order harmonics are lower than the odd-order harmonics. The fact that the power in the harmonic tones decreases very rapidly is related to using a differential active inductor topology. There is more harmonic content in the 1-GHz oscillator in Fig. 11 than in the 2-GHz oscillator because the OTAs in the 1-GHz oscillator were biased at a lower bias voltage, and therefore, there was less voltage headroom in the active inductor. This, in turn, leads to more signal distortion that manifests itself as more energy in the harmonic tones.

A measurement of the power in the fundamental (1st), second (2nd), and third (3rd) harmonics as a function of OTA bias voltage V_{gm} was carried out, and the results are plotted in Fig. 13. In addition, the simulation results for the fundamental output power are also included for comparison purposes. The measured fundamental output power varies between -0.9 and -5 dBm, whereas the 2nd and 3rd harmonics are below -41 and -27 dBm, respectively.

The measured phase noise of the oscillator at a 1-MHz offset from a carrier of 1.26 GHz was -104 dBc/Hz. When the carrier was increased to 2.43 GHz, the phase noise was -109 dBc/Hz at a 1-MHz offset. The phase noise plots for the 1.26- GHz and 2.43-GHz cases are shown in Fig. 14.

The circuit is biased from a single 1.2-V supply. The power consumption of the core oscillator is from 8 to 13 mW. The buffer circuits used to interface the oscillator with off-chip test and measurement equipment consumed an additional power of 15.6 mW. A photograph of the fabricated chip is shown in Fig. 15.

A comparison between this brief and recent active inductor-based VCOs that reported measured results is shown in Table I. The oscillator presented in this brief has the highest output power and the best dc-to-RF output power efficiency.

V. CONCLUSION

An active inductor-based VCO has been presented in this brief. The differential active inductor, with resistance feedback, consists of two high-linearity high-speed OTAs and achieves a wider inductance tuning range than the conventional one. The resulting circuit had a very wide tuning range and high dc-to-RF output power efficiency. The power in the even harmonics was much reduced because of the differential nature of the active inductor circuit.

REFERENCES

[1] J. Laskar, R. Mukhopadhyay, and C.-H. Lee, "Active inductor-based oscillator: A promising candidate for low-cost low-power multi-standard signal generation," in *Proc. IEEE Radio Wireless Symp.*, Jan. 2007, pp. 31–34.

[2] L.-H. Lu, H.-H. Hsieh, and Y.-T. Liao, "A wide tuning-range CMOS VCO with a differential tunable active inductor," *IEEE Trans. Microw. Theory Tech.*, vol. 54, no. 9, pp. 3462–3468, Sep. 2006.

[3] R. Mukhopadhyay, Y. Park, P. Sen, N. Srirattana, J. Lee, C.-H. Lee, S. Nuttinck, A. Joseph, J. D. Cressler, and J. Laskar, "Reconfigurable RFICs in Si-based technologies for a compact intelligent RF front-end," *IEEE Trans. Microw. Theory Tech.*, vol. 53, no. 1, pp. 81–93, Jan. 2005.

[4] Y. Wu, M. Ismail, and H. Olsson, "CMOS VHF/RF CCO based on active inductors," *Electron. Lett.*, vol. 37, no. 8, pp. 472–473, Apr. 2001.

[5] F. Yuan, *CMOS Active Inductors and Transformers: Principle, Implementation, and Applications*. New York: Springer-Verlag, 2008.

[6] C.-C. Hsiao, C.-W. Kuo, C.-C. Ho, and Y.-J. Chan, "Improved quality-factor of 0.18-μm CMOS active inductor by a feedback resistance design," *IEEE Microw. Wireless Compon. Lett.*, vol. 12, no. 12, pp. 467–469, Dec. 2002.

[7] K. S. Hwang, C. S. Cho, J. Lee, and J. Kim, "High quality-factor and inductance of symmetric differential-pair structure active inductor using a feedback resistance design," in *Proc. IEEE MTT-S Int. Microw. Symp. Dig.*, 2008, pp. 1059–1062.

[8] Y. Zheng and C. Saavedra, "Full 360° vector-sum phase-shifter for microwave system applications," *IEEE Trans. Circuits Syst. I, Reg. Papers*, vol. 57, no. 4, pp. 752–758, Apr. 2010.

[9] Y. Zheng and C. E. Saavedra, "Feedforward-regulated cascode OTA for gigahertz applications," *IEEE Trans. Circuits Syst. I, Reg. Papers*, vol. 55, no. 11, pp. 3373–3382, Dec. 2008.

[10] J. Xu, C. Saavedra, and G. Chen, "Wideband microwave ota with tunable transconductance using feedforward regulation and an active inductor load," in *Proc. 8th IEEE Int. NEWCAS Conf.*, 2010, pp. 93–96.

[11] Y.-T. Liao and C.-J. Shi, "A 6–11ghz multi-phase vco design with active inductors," in *Proc. IEEE ISCAS*, May 2008, pp. 988–991.